Published in final edited form as:
Neurobiol Aging. 2012 April ; 33(4): 826.e15–826.e30. doi:10.1016/j.neurobiolaging.2011.06.006.

Phosphorylation in the amino terminus of tau prevents inhibition of anterograde axonal transport

Nicholas M. Kanaan[a,b], **Gerardo Morfini**[b,c], **Gustavo Pigino**[b,c], **Nichole E. LaPointe**[d], **Athena Andreadis**[e], **Yuyu Song**[b,c], **Ellen Leitman**[b], **Lester I. Binder**[f,g], and **Scott T. Brady**[b,c,g]

[a]Division of Translational Science and Molecular Medicine, Michigan State University, Grand Rapids, MI 49503, USA

[b]Marine Biological Laboratory, Woods Hole, Massachusetts 02543, USA

[c]Department of Anatomy and Cell Biology, University of Illinois at Chicago, Chicago, Illinois 60607, USA

[d]Neuroscience Research Institute, University of California, Santa Barbara, California 93106, USA

[e]Department of Cell Biology, University of Massachusetts Medical School, Worcester, Massachusetts 01655, USA

[f]Department of Cell and Molecular Biology, Feinberg School of Medicine, Northwestern University, Chicago, Illinois 60611, USA

Abstract

Alzheimer's disease (AD) and other tauopathies are characterized by fibrillar inclusions composed of the microtubule-associated protein, tau. Recently, we demonstrated that the N-terminus of tau (aa 2–18) in filamentous aggregates or N-terminal tau isoforms activates a signaling cascade involving protein phosphatase 1 and glycogen synthase kinase 3 that results in inhibition of anterograde fast axonal transport (FAT). We have termed the functional motif comprised of aa 2–18 in tau the phosphatase-activating domain or PAD. Here, we show that phosphorylation of tau at tyrosine 18, which is a fyn phosphorylation site within PAD, prevents inhibition of anterograde FAT induced by both filamentous tau and 6D tau. Moreover, Fyn-mediated phosphorylation of tyrosine 18 is reduced in disease-associated forms of tau (e.g. tau filaments). A novel PAD-specific monoclonal antibody revealed that exposure of PAD in tau occurs before and more frequently than tyrosine 18 phosphorylation in the evolution of tangle formation in AD. These results indicate that N-terminal phosphorylation may constitute a regulatory mechanism that controls tau-mediated inhibition of anterograde FAT in AD.

Corresponding author: Scott T. Brady, PhD, University of Illinois at Chicago, Department of Anatomy and Cell Biology, 808 S. Wood St. Rm 578 (M/C 512), Chicago, IL 60612, Phone: (312) 996-6791, FAX: (312) 413-0354, stbrady@uic.edu.
[g]S.T.B. and L.I.B contributed equally to this work.

Disclosure statement
NMK, GM, STB, LIB and NEL are co-inventors on a pending patent for targeting PAD as therapeutic intervention for Alzheimer's disease and other tauopathies. The authors have no other actual or potential conflicts of interest to report.

Appendix A. Supplementary data
Supplementary data includes supplementary methods and four figures, which can be found with this article online.

Keywords

Alzheimer's disease; fyn kinase; axonal transport; tau filaments; tauopathy; protein phosphatase; glycogen synthase kinase; kinesin; tyrosine phosphorylation

1. Introduction

Tau is the major constituent of the fibrillar pathologies that characterize Alzheimer's disease (AD) and other tauopathies (Pollock et al., 1986). The accumulation of tau inclusions correlates with progressive cognitive decline in AD (Giannakopoulos et al., 2003). Furthermore, *tau* gene mutations cause familial frontotemporal dementias, directly implicating tau in disease pathogenesis (Goedert and Jakes, 2005). Despite the clear association between tau, cognitive decline and neurodegeneration, the mechanisms through which tau elicits neuronal dysfunction remain elusive.

Defects in fast axonal transport (FAT) represent a plausible mechanism for early synaptic dysfunction that is characteristic of AD and tauopathies (Morfini et al., 2009a; Roy et al., 2005). Hallmarks of dying back neuropathies such as neuritic swellings, organelle and protein mislocalization, and synaptic dysfunction have been reported in AD and AD animal models (Price et al., 1997). Recently, we reported that physiological levels of tau filaments disrupt FAT (LaPointe et al., 2009). Specifically, filamentous tau aggregates inhibited kinesin-dependent anterograde FAT in isolated squid axoplasm, while monomeric tau had no effect. The inhibitory effect of filamentous tau was driven by the activation of a signaling cascade involving protein phosphatase 1 (PP1) and glycogen synthase kinase 3 (GSK3), which in turn phosphorylated kinesin light chains and promoted the dissociation of kinesin from its cargo (LaPointe et al., 2009; Morfini et al., 2004; Morfini et al., 2002b). This effect was dependent upon the availability of aa 2–18, termed the phosphatase-activating domain (PAD) of tau (Kanaan et al., in preparation, 2011). Thus, biochemically heterogeneous modifications in tau (i.e. filament formation, truncation, hyperphosphorylation, etc.) that increase PAD exposure can result in anterograde FAT inhibition.

The abundance of tau in neurons and the ability of some neurons to survive for several decades in the presence of tau inclusions (Morsch et al., 1999) suggest that mechanisms exist that allow neurons to counteract the toxic effects of tau filaments on FAT. Phosphorylation is a plausible mechanism since tau is a well-known phosphoprotein that becomes abnormally phosphorylated in disease (Iqbal et al., 2005). Most tau phosphorylation sites are Ser/Thr sites, but four of the five tyrosines in tau (Y18, 29, 197, and 394) have been identified as targets of non-receptor tyrosine kinase (Lebouvier et al., 2009). Among these, fyn is a non-receptor tyrosine kinase that phosphorylates Y18 in tau (Lee et al., 2004), and fyn levels are increased in tangle-bearing neurons in AD brains (Ho et al., 2005). However, the effect of Y18 phosphorylation on tau toxicity is unknown.

Here, we report that N-terminal phosphorylation of tau at Y18 prevents PAD from activating the PP1-GSK3 signaling cascade, thereby preventing its inhibitory effect on FAT. We also present data suggesting that certain disease-associated forms of tau are not as readily phosphorylated by fyn kinase. A novel antibody recognizing PAD (TNT1) and a phosphoY18-specific antibody show that PAD exposure precedes and exceeds Y18 phosphorylation during AD progression. Together, these data provide compelling evidence suggesting a functional role for Y18 phosphorylation in regulating the inhibitory effect of PAD on anterograde FAT in AD and other tauopathies.

2. Methods

2.1. Recombinant tau proteins

The amino acid numbering used for the recombinant tau proteins (Fig. 1) is based on the largest adult human isoform (ht40; 441 amino acids) in the central nervous system. Full-length wild-type ht40 (WT tau) and the non-canonical N-terminal 6D isoform of tau were generated from the previously described pT7c plasmid cDNAs (LaPointe et al., 2009; Luo et al., 2004). Site-directed mutagenesis (Stratagene, QuickChange II Kit, 200524) was used to create point mutations in tau constructs. Tyrosine (Y) and threonine (T) residues were mutated to glutamic acid (E) to create pseudophosphorylation mutants (Y→E). Mutations to phenylalanine (Y→F) were used as control constructs for the Y→E constructs. A tau construct in which all of the Y residues (Y29, Y197, Y310 and Y394), except Y18, were mutated to F was created to ensure fyn kinase phosphorylation was specific to Y18 (see below). Serine 199, S202, and T205 were mutated to glutamic acid (E) to create the AT8 pseudophosphorylated mutant protein (AT8 tau). Deletion of amino acids 144–273 (Δ144–273 tau) was done by inserting EcoRV restriction sites flanking the appropriate region of the cDNA. Following EcoRV digestion and T4 ligation (New England Biolabs; according to manufacturer's instructions), the remaining EcoRV site was removed via deletion using the site-directed mutagenesis kit described above. The plasmid cDNAs containing the tau constructs were amplified in XL-1 blue supercompetent *E. coli* cells, purified using the Qiagen Miniprep kit, and verified by DNA sequencing. Tau proteins were expressed in T7 express supercompetent *E. coli* cells and purified through his-tag high affinity resin and size exclusion chromatography as described previously (Carmel et al., 1996).

2.2. Tau polymerization reaction

Tau proteins were polymerized into filamentous aggregates as previously described using arachidonic acid as the inducer (LaPointe et al., 2009). Briefly, 4μM tau protein (WT tau, Y18E tau, Y18F tau, Y29E tau or pY18 tau) was incubated at room temperature in polymerization buffer (50mM HEPES, 50mM KCl, 0.1mM EDTA and 5mM DTT; pH 7.6) with arachidonic acid (75μM) for 5 hours to generate tau filament. The same protocol was used to make tau monomer samples, but arachidonic acid was omitted. A combination of laser light scattering and electron microscopy was used to monitor the extent and characteristics of polymer formation.

2.3. Laser light scattering assay (LLS)

The polymerization reactions for full-length tau proteins were monitored using a laser light scattering assay as previously described (Gamblin et al., 2000). Polymerization of WT, Y18E, Y18F, Y29E and pY18 tau proteins (250 μl volume) was monitored by measuring the intensity of scattered light (I_s) 90° to the incident light. Images of the scattered light were captured throughout the 5-hour polymerization reaction using a digital camera. The intensity of scattered light was measured in Photoshop as described previously (Gamblin et al., 2000).

2.4. Electron microscopy

Aliquots of polymerized samples were fixed with 2% gluteraldehyde, spotted on carbon-coated Formvar grids, stained with 2% uranyl acetate, and visualized using a JEOL 1220 transmission electron microscope as previously described (Gamblin et al., 2000).

2.5. Generation of Y18 phosphorylated tau filaments

To obtain full-length tau polymers with phosphorylated Y18 residues, tau containing a single Y residue at position 18 (Y4F tau) was phosphorylated by fyn kinase prior to polymerization. Y4F tau monomers (4 μM) were incubated with active fyn kinase (0.21U/

μM tau; Millipore, 14–441) for 5 hours at 32° C in phosphorylation-polymerization buffer (50mM HEPES, 50mM KCl, 5mM $MgSO_4$, 0.1mM EDTA and 5mM DTT; pH 7.6) supplemented with 1mM ATP. Then the samples were heated to 99° C for 20 minutes to inactivate the fyn kinase. Samples were cooled on ice for 20 minutes and then polymerized as described above with arachidonic acid inducer (75μM) for 5 hours. The resulting filaments composed of tau phosphorylated at Y18 (pY18 filaments) were used in the squid axoplasm motility assay described below. Aliquots of polymerized pY18 tau were processed for electron microscopy as described above. Preliminary experiments determined that phosphorylation at Y18 by fyn kinase reached saturation within 1 hour (Supplementary Fig. S2).

2.6. Squid axoplasm motility assay

Fast axonal transport was measured using vesicle motility assays in extruded axoplasm from the squid giant axon (*Loligo pealii*; Marine Biological Laboratory, Woods Hole, MA) as previously described (Brady et al., 1993; Morfini et al., 2002b). Tau proteins (2μM; monomers or filaments) in X/2 buffer (175mM potassium aspartate, 65mM taurine, 35mM betaine, 25mM glycine, 10mM HEPES, 6.5mM MgCl2, 5mM EGTA, 1.5mM CaCl2, 0.5mM glucose, 10mM ATP, pH 7.4) were perfused into extruded axoplasms. Tau proteins (2μM) were perfused within the physiological ranges of tau monomer:tubulin dimer (LaPointe et al., 2009; Morfini et al., 2007a). Vesicle motility in the axoplasm was visualized using a Zeiss Axiomat microscope with a 100X objective (1.3 N.A.) and DIC optics. Transport in the anterograde and retrograde directions were measured by matching vesicle speed with calibrated cursors and vesicle motility was monitored for 50 minutes after perfusion.

2.7. In vitro phosphorylation of tau by fyn kinase

Full-length tau monomers (1μM) or filaments (1μM) were incubated with active fyn kinase (0.05U/μM tau; Millipore, 14–441) as described above for 60 minutes. The samples were diluted 1:1 in 2X Laemmli buffer at 0, 5, 10, 15, 20, 30, 40, 50 and 60 minutes to stop the reaction and then were analyzed by immunoblotting or ELISA. To ensure phosphorylation at Y18 occurred in tau incorporated into the filaments, a spin down assay was performed. Briefly, tau monomers (M) or filaments (F) were phosphorylated as described above for 10 minutes. An aliquot of each sample was taken before incubation with fyn kinase as the non-phosphorylated samples (NonPh). Following phosphorylation, an aliquot was taken from each sample as the phosphorylated pre-spin samples (Ph). The remaining samples were layered over a 40% glycerol cushion and centrifuged at 355,040×g for 45 minutes at 25° C. The soluble tau proteins not incorporated into filaments were collected in the supernatant (S) and pelleted tau filaments were collected (P). The samples were diluted 1:1 in 2X sample buffer and analyzed using immunoblotting.

Wild-type tau, AT8 tau, or Δ144–273 tau (1μM each) monomers were incubated with active fyn kinase (0.05U/μM tau) as described above for 180 minutes. Sample aliquots were diluted 1:1 in 2X Laemmli buffer at 0, 10, 20, 40, 60, 120 and 180 minutes to stop the reaction. Samples were stored at −20° C until used for immunoblotting or ELISA.

2.8. Immunoblotting

Samples in Laemmli buffer were heated to 60° C for 5 minutes and proteins were separated via SDS-PAGE (10% gels). The proteins were transferred to nitrocellulose membranes, blocked in 2% non-fat dry milk tris buffered saline (NFDM-TBS; Tris 50mM, NaCl 150mM, pH 7.4). The membranes were incubated overnight at 4° C in appropriate primary antibodies (R1–1:300,000; Tau7–1:1,000,000; 9G3-1:8000). The 9G3 antibody (supplied as culture supernatant) was a generous gift from Dr. Gloria Lee (Lee et al., 2004). The R1 tau

(polyclonal) and Tau7 (C-terminal epitope) antibodies have been described previously (Berry et al., 2004; Horowitz et al., 2006). After incubating in primary antibodies, the membranes were rinsed in TBS + 0.1% Tween 20 and then incubated in appropriate secondary antibody (1:5000 in 2% NFDM-TBS; Vector, PI-2000 and PI-1000). The membranes were rinsed and reactivity was visualized using ECL solution (Pierce, 32106). The level of reactivity was determined by measuring the optical density (average pixel intensity) of the main tau band using ImageJ software (v1.41, NIH). Data are expressed as the ratio of 9G3 intensity (pY18 tau) to R1 intensity (total tau). Antibodies were appropriately titered to ensure usage within the linear range of reactivity.

2.9. Enzyme-linked immunosorbent assay (ELISA)

Samples of WT tau, AT8 tau and Δ144–273 tau from the *in vitro* phosphorylation experiments were used to coat high binding 96 well plates (6nM tau/well) for 1 hour at room temperature. The wells were rinsed and then incubated with either Tau 7 antibody (1:25,000) or 9G3 antibody (1:500) for 2 hours at room temperature. Each antibody was pre-titered to ensure usage within the linear range of reactivity. After rinsing, the wells were incubated with peroxidase conjugated goat anti-mouse secondary antibody (1:2500) for 1 hour at room temperature. Immunoreactivity was developed using 3,3', 5,5'-tetramethylbenzidine (TMB), the reaction was stopped with 3% sulfuric acid, and absorbance was measured at 450 nm using a microplate reader. Data are expressed as the ratio of 9G3 to Tau7 absorbance units at 450nm (error bars = +SEM).

2.10. Tau N-terminus 1 (TNT1) antibody generation and characterization

The monoclonal TNT1 antibody (IgG1) was generated by immunizing BALB/c female mice with a synthetic PAD peptide (C^{2}AEPRQEFEVMEDHAGTY^{18}) conjugated to KLH (GenScript, Piscataway, NJ) as previously described (Reyes et al., 2008). Clones that reacted specifically with PAD by ELISA analysis were selected and then subcloned four times prior to antibody production and purification as described (Reynolds et al., 2006).

The TNT1 antibody was tested in immunoblots with WT tau and Δ2–18 tau to test for PAD specificity. In addition, TNT1 was tested against Y4F tau and pY18 Y4F tau (see above) in immunoblots to determine whether Y18 phosphorylation affects TNT1 binding. The recombinant proteins were analyzed in Western blots as outlined below. Lastly, soluble tau (representing normal tau) and sarkosyl insoluble tau (representing paired helical filament) fractions were extracted from fresh frozen frontal cortex tissue of 3 control and 3 AD cases (obtained from the Brain Bank of the Cognitive Neurology and Alzheimer's Disease Center at Northwestern University) following a similar protocol as previously described (Hasegawa et al., 1992). Soluble and insoluble tau samples were run in both Western (denaturing conditions) and dot blots (non-denaturing conditions). All of the membranes were probed with TNT1 (1:200,000) and R1 tau (1:50,000, total tau) antibodies and detected with goat anti-mouse IRDye 680LT (Licor, 926–68020) and goat anti-rabbit IRDye 800CW (Licor, 926–3224), respectively. Image acquisition and intensity measurements were performed with a Licor Odyssey imaging system. Data are presented as the ratio of TNT1 to R1 integrated intensity values.

2.11. TNT1 and 9G3 double-label immunohistochemistry

Tissue sections (40μm thick) from the hippocampus of control (Braak stages I–II; n=4), mild AD (Braak stages III–IV; n=4) and severe AD (Braak stages V–VI; n=4) cases were obtained through the Cognitive Neurology and Alzheimer's Disease Center at Northwestern University. All sections were stained simultaneously to reduce variability in tissue processing. The standard steps for tissue staining (e.g. blocking, peroxidase quenching, ABC kit, rinsing, etc.) were performed as previously described (Kanaan et al., 2007). The TNT1

primary antibody (see Kanaan et al., in preparation, 2011, for detailed description) was diluted 1:400,000 (from 1mg/ml stock) and incubated with the tissue sections overnight at 4° C. The tissue was incubated in biotinylated goat anti-mouse secondary antibody (Vector, BA-9 200, diluted 1:500) for 2 hours. The staining was developed with 3,3′-diaminobenzidine (Sigma, D5637), which creates a brown chromogen. Following development of TNT1 staining, remaining peroxidase activity was quenched with 3% H_2O_2 for 1 hour, uncomplexed binding sites on the secondary antibodies were blocked with 5% mouse serum, and then available binding sites on mouse IgGs were blocked with goat anti-mouse Fab fragments (Jackson Immunoresearch, 115-007-003, diluted 1:500). Avidin-biotin complexes from the TNT1 stain were blocked using the Avidin/Biotin blocking kit (Vector, SP-2001, according to manufacturer's instructions). The tissue sections were next incubated in 9G3 primary antibody (diluted 1:250) overnight at 4° C, followed by the goat anti-mouse secondary antibody as above, and then developed using the Vector SG kit (Vector, SK4700), which produces a blue/gray chromogen. Images were taken using a Nikon Eclipse 90i microscope equipped with a DS-Ri1 camera and Nikon Elements AR 3.10 software. Figures were generated using Adobe Photoshop.

2.12. TNT1 and 9G3 double-label immunofluorescence

Tissue sections (as described above) from the hippocampus of control (Braak stages I–II; n=4), mild AD (Braak stages III–IV; n=5) and severe AD (Braak stages V–VI; n=4) cases were processed for double-label immunofluorescence using TNT1 (IgG1) and the 9G3 (IgG2a) antibody. All sections were stained simultaneously to reduce variability in tissue processing, which was done according to previous methods (Kanaan et al., 2007). The tissue was incubated overnight at 4° C in a primary antibody solution containing TNT1 (1:40,000) and 9G3 (1:200) antibodies. Then the tissue was incubated in a secondary antibody solution containing Alexa Fluor 594 goat anti-mouse IgG1-specific secondary antibody (Invitrogen, A21125, diluted 1:500) and Alexa Fluor 488 goat anti-mouse IgG2a-specific secondary antibody (Invitrogen, A21131, 1:300) for 2 hours. All steps were done at room temperature unless otherwise noted and each step was followed by rinses (6 × 10 minute in TBS-0.5% Triton X-100). Images were taken using a fluorescence equipped Nikon Eclipse 90i microscope with a Q-imaging Retiga-SRV Fast1394 camera and Nikon Elements AR 3.10 software (with live de-blur function). Figures were generated using Adobe Photoshop.

2.13. Statistics

Each experiment was repeated three to five times (see figures). Comparisons of vesicle motility rates were made using a one-way ANOVA test. The immunoblotting results were analyzed with either a two-way repeated measure ANOVA test or a two-way ANOVA test where appropriate. When overall significance was reached, the Student-Newman-Keuls *post hoc* analysis was used to make all possible comparisons. Significance was set at $p<0.01$ or $p<0.05$, as noted. Sigmastat software (Systat Software, Inc., San Jose, CA) was used for all statistical tests.

3. Results

3.1. Y18 Pseudophosphorylation prevents tau filaments from inhibiting anterograde FAT

Our previous work evaluated the effects of tau on FAT using vesicle motility assays in isolated squid axoplasm (LaPointe et al., 2009; Morfini et al., 2007a). This *ex vivo* model system allows for a direct, quantitative evaluation of different effectors on anterograde (conventional kinesin-dependent) and retrograde (cytoplasmic dynein-dependent) FAT rates by video microscopy (Brady et al., 1993). Isolated axoplasm has been used to examine effects of numerous pathogenic proteins, including huntingtin (Morfini et al., 2009b), spastin (Solowska et al., 2008), amyloid-β (Pigino et al., 2009), superoxide dismutase type 1 (Bosco

et al., 2010), and MPTP/MPP+ (Morfini et al., 2007b). In each case, the results obtained in isolated axoplasms were confirmed in mammalian models.

In isolated axoplasm, tau filaments, but not soluble monomers, selectively inhibit anterograde FAT through PAD-dependent activation of the PP1-GSK3 cascade, kinesin light chain phosphorylation, and cargo dissociation from kinesin-1 (LaPointe et al., 2009; Morfini et al., 2004). *In vitro*, recombinant wild-type (WT) tau (Fig. 1A) was assembled into filaments (Fig. 2A) that structurally resemble those found in AD brains (King et al., 1999). Consistent with our previous work (LaPointe et al., 2009; Morfini et al., 2007a), recombinant tau monomers had no effect on FAT (Fig. 2B and G) in isolated squid axoplasm. In contrast, tau filaments caused a significant and selective reduction in the rate of anterograde FAT (Fig. 2C and G).

PAD is necessary and sufficient for anterograde FAT inhibition (Kanaan et al., in preparation 2011), and here we evaluate the role of N-terminal phosphorylation in modulating this effect. The primary N-terminal phosphorylation sites, Y18 and Y29, are substrates for non-receptor tyrosine kinases (Lee et al., 2004). Several pseudophosphorylation tau mutants were generated using site-directed mutagenesis (Fig. 1B). Both Y18 (within PAD) and Y29 (adjacent to PAD) were mutated to glutamic acid (E) to mimic the negative charge and conformational effects of phosphorylation. As a non-phosphomimicking mutation control, Y→F (phenylalanine) tau mutants were generated. Laser light scattering (Supplementary Fig. S1A) and electron microscopy (Fig. 2A) confirmed that all tau mutant proteins polymerize into filaments morphologically indistinguishable from those assembled from WT tau, as previously reported (Reynolds et al., 2005).

The effect of pseudophosphorylated tau mutants on FAT was evaluated using vesicle motility assays in isolated squid axoplasm. Y18E tau filaments had no effect on FAT in either direction (Fig. 2D and G). In contrast, Y18F tau filaments selectively inhibited anterograde FAT, just like WT tau filaments (Fig. 2E and G). Y18F tau monomers were tested to ensure that inhibition induced by Y18F tau filaments was not a result of the Y→F mutation, rather than being due to their filamentous conformation. As predicted, monomeric Y18F tau had no effect on FAT (Supplementary Fig. S1B). Next, Y29E tau filaments were used to examine whether modifying a site downstream from PAD would affect tau filament-induced FAT inhibition. Y29E mutant tau filaments reduced the rate of anterograde FAT (Fig. 2F and G) much like WT tau filaments. Neither WT nor any mutant tau filament significantly affected retrograde FAT ($p>0.01$; Fig. 2G). Together, these data indicate that Y18 phosphorylation within PAD abolished the deleterious effect of filamentous tau on anterograde FAT, suggesting that Y18 phosphorylation blocks activation of the PP1-GSK3 signaling cascade by PAD.

3.2. Fyn-phosphorylated tau filaments do not affect FAT

Next, we sought to determine whether addition of a bona fide phosphate group at Y18 would have the same effect as Y18 pseudophosphorylation. The non-receptor tyrosine kinase fyn is known to phosphorylate Y18 in human tau, and a subset of tau inclusions found in AD brains contains phosphorylated Y18 tau (Lee et al., 2004). Therefore, we used recombinant fyn kinase to phosphorylate a tau mutant containing only Y18 (Fig. 1C) prior to polymerization into filaments. Fyn kinase rapidly phosphorylated the Y18 mutant tau (pY18 tau) to saturation by 1 hour (Supplementary Fig. S2). Electron microscopic analysis showed that Y18 phosphorylation did not inhibit *in vitro* filament assembly (pY18 filaments; Fig. 3A) and immunoblotting with a phosphorylated Y18-specific antibody (9G3) (Lee et al., 2004) confirmed phosphorylation on Y18 (Fig. 3B). In isolated axoplasms, FAT was not affected in either direction by pY18 filaments (Fig. 3C and D). These data validated results

obtained using pseudophosphorylated tau filaments (Fig. 2B–G), and suggested that fyn-mediated Y18 phosphorylation may represent a novel mechanism through which tau filaments can be rendered non-toxic in AD and other tauopathies.

3.3. Fyn differentially phosphorylates filamentous and monomeric tau

Phosphorylation of Y18 abolished the inhibitory effect of tau filaments on FAT, but it remained unclear whether tau that was already incorporated into filaments could be phosphorylated at Y18 by fyn. *In vitro* kinase assays and quantitative immunoblotting were used to determine the ability of recombinant fyn kinase to phosphorylate Y18 in preformed tau filaments. Y18 was phosphorylated to a greater extent in tau monomers than in tau filaments after 10, 15, 20 and 30 minutes of incubation with fyn kinase (Fig. 4A and B). The rate of Y18 phosphorylation for tau monomers ($t½$ = 11.88 min ±2.99) was approximately twice as fast as that for tau filaments ($t½$ = 22.91 min ±4.86); however, the maximal level of pY18 reactivity was similar between tau monomers (1.11 ±0.02) and filaments (0.99 ±0.03) (Fig. 4B). Electron microscopy confirmed that a similar amount of tau filaments was present after 0 and 60 minutes of incubation with fyn kinase (Fig. 4C). These data suggest the presence of tau in the filamentous form reduces the efficiency of fyn kinase phosphorylation at Y18.

To confirm whether fyn kinase added phosphates onto tau incorporated into filaments, and not simply to monomers in the reaction mixture, a centrifugation assay of tau filaments phosphorylated for 10 minutes (the greatest difference between monomers and filaments) was performed. Pelleted filaments contained pY18 tau (Fig. 4D), and the relative level of pY18 in pelleted filaments was approximately 40% below those of the soluble, unpolymerized monomers in the reaction (Fig. 4E). As expected, no tau was detected in the pellet fraction when phosphorylated tau monomers were subjected to centrifugation as a control (Fig. 4D and E). These data confirm a significant reduction in the rate of Y18 phosphorylation by fyn kinase in filamentous tau.

Finally, we sought to determine whether endogenous non-receptor tyrosine kinases in squid axoplasm differentially phosphorylated tau monomers and tau filaments (Supplementary materials and methods). Immunoblotting experiments showed near-background levels of pY18 tau for both tau monomers (1μM) and filaments (1μM) after incubation with isolated squid axoplasms (Supplementary Fig. S3), suggesting that endogenous squid tyrosine kinases do not readily phosphorylate Y18, which may reflect low levels of active fyn kinase in squid axoplasm.

3.4. Fyn-mediated phosphorylation of Y18 is reduced in disease-associated tau species

To determine whether fyn-mediated phosphorylation of Y18 is affected by conformational tau changes associated with pathology, we examined the ability of fyn to modify two disease-associated forms of tau. In the first, tau was pseudophosphorylated at S199, S202, and T205 to mimic the AT8 antibody epitope (AT8 tau, Fig. 1D) (Jeganathan et al., 2008), which correlates with early AD pathology (Braak et al., 1994). A second tau construct was made in which amino acids 144–273 were deleted (Δ144–273 tau; Fig. 1E), which mimics a tau mutation found in an inherited form of frontotemporal dementia (FTD) (Rovelet-Lecrux et al., 2009). The Δ144–273 tau mutant exhibits substantially reduced microtubule binding (Rovelet-Lecrux et al., 2009) and reduced filament formation *in vitro* (N Kanaan and L Binder, unpublished data, 2011).

The level of Y18 phosphorylation in WT and mutant tau monomers was visualized by immunoblotting (Fig. 5A) and quantified using an ELISA (Fig. 5B). When compared to WT tau, AT8 tau had a significantly slower rate of phosphorylation at Y18 ($t½$: WT tau = 33.62

min. and AT8 tau = 83.11 min), but a similar maximal level (Maximum: WT tau = 1.05 ±0.02; AT8 tau = 1.09 ±0.01) (Fig. 5B). The FTD construct, Δ144–273 tau, had a much slower rate and lower maximal level of phosphorylation at Y18, such that both measures were indeterminate (Fig. 5B). These data suggest that a mechanism capable of preventing inhibition of anterograde FAT by pathogenic forms of tau (e.g. Y18 phosphorylation by fyn) can be impaired either by abnormal phosphorylation at the AT8 sites or by deletion of residues 144–273 in tau.

3.5. Y18 phosphorylation prevents PAD-mediated FAT inhibition independent of effects on tau folding

Phosphorylation at Y18 by fyn prevented inhibition of anterograde FAT by filamentous tau; however, two mechanistic explanations were possible: 1) The phosphate modification could directly block the toxic action of PAD by steric hindrance/charge repulsion, or 2) The modification could affect folding of tau within filaments. To distinguish between these possibilities, we used the short 6D isoform of tau that lacks the proline rich region, MTBRs and the carboxy terminus of WT tau (Fig. 1F), but still inhibits anterograde FAT (LaPointe et al., 2009). Since 6D inhibits anterograde FAT as a monomer (6D cannot form filaments), we concluded that PAD was constitutively exposed in the context of this isoform. Thus, 6D allowed us to study the effects of the N-terminus independent of aggregation, microtubule binding, and other functional elements of tau (Luo et al., 2004). If pseudophosphorylation of residues within PAD abrogate the inhibitory effect of 6D tau on anterograde FAT, it would suggest that phosphorylation of PAD physically (steric hinderance or charge repulsion) blocks activation of the PP1-GSK3 pathway.

Using site-directed mutagenesis, pseudophosphorylated (Y→E or T→E) 6D tau mutants were generated bearing mutations at Y18, T17 or Y29 (Fig. 1G). We perfused isolated axoplasm with WT 6D tau and pseudophosphorylated 6D tau mutant monomers (Fig. 6). As previously shown (LaPointe et al., 2009), WT 6D tau caused a significant reduction in anterograde, but not retrograde FAT (Fig. 6A and E). Consistent with results obtained with full-length Y18E tau filaments, FAT was unaffected in isolated axoplasm perfused with Y18E 6D tau (Fig. 6B and E). The non-phosphomimicking mutation control, Y18F 6D tau, caused a significant reduction in anterograde, but not retrograde FAT (Fig. 6C and E) suggesting that the change in charge caused by the Y→E substitution *within PAD* was responsible for the loss of FAT inhibition with Y18E 6D tau. We tested a T17E 6D tau construct where the threonine also lies within PAD to test whether modifications need to be within PAD to affect FAT inhibition. As predicted, the T17E 6D tau prevented FAT inhibition (Fig. 6E and Supplementary Fig. S4). Pseudophosphorylation of 6D tau at Y29, which is slightly downstream of PAD, only partially prevented inhibition of anterograde FAT (~40% less prevention than Y18E) (Fig. 6D and E). Together, these data confirm that exposure of PAD is required to inhibit FAT, and that this process may be regulated through phosphorylation within or near PAD.

3.6. PAD exposure and Y18 phosphorylation in human brains

To evaluate the relationship between PAD exposure and Y18 phosphorylation in human disease, a novel PAD-specific monoclonal antibody (TNT1) and pY18 tau-specific antibody (9G3, (Lee et al., 2004)) were used. We confirmed that TNT1 is specific for PAD (aa 2–18) and that Y18 phosphorylation does not affect TNT1 binding using recombinant tau proteins (Fig. 7A). The TNT1 antibody labels the typical pattern of tau proteins isolated from the human brains (Fig. 7B). When used in *denaturing conditions* (Western blot), TNT1 reacts similarly with soluble and insoluble tau fractions isolated from the frontal cortex of control and AD human patients (Fig. 7B). In contrast, when TNT1 is used in *non-denaturing conditions* (dot blot), it shows remarkable selectivity for soluble and insoluble tau isolated

from AD brains, as opposed to controls (Fig. 7C). These data indicate that PAD is more available in the native state of AD tau and that TNT1 immunoreactivity is indicative of PAD exposure.

Qualitative immunohistochemical analysis in hippocampal sections revealed that, in the early stages of tau accumulation (diffuse TNT1 stained neurons), tau is not phosphorylated at Y18 in control brains (Braak stages I–II) (Fig. 7D and E); however, nearly all neurons containing seemingly more mature compact tau inclusions were positive for both TNT1 and 9G3 (Fig. 7D). Compared to controls, the amounts of TNT1 positive pathology and TNT1+9G3 double-labeled tau inclusions were increased, but 9G3 staining was increased to a lesser extent than TNT1 in mild and severe AD cases (Fig. 7F). The co-localization between TNT1 and 9G3 is apparent in double-label immunohistochemistry stains (Fig. 7G–I), and was confirmed using double-label immunofluorescence (Fig. 7J–M). Both TNT1 and 9G3 labeled the triad of AD tau pathology, the neurofibrillary tangles, neuropil threads and neuritic plaques (Fig. 7). Most neuritic plaques contained a combination of TNT1 only and TNT1+9G3 double stained components in mild and severe AD cases. Cells labeled only by 9G3 occurred rarely or not at all in the cases analyzed. These data demonstrate that PAD exposure occurs prior to phosphorylation at Y18 during the progression of AD. In addition, there is a large fraction of exposed PAD that is not phosphorylated at Y18 in mild and severe AD.

4. Discussion

Our previous work (LaPointe et al., 2009) established that the N-terminus of tau was required for filamentous tau aggregates to initiate a PP1-GSK3 cascade that led to inhibition of anterograde FAT. Additional studies indicated these effects involved increased exposure of a functional domain we termed the phosphatase-activating domain or PAD. Using phosphorylated tau and pseudophosphorylation tau mutants, we demonstrated that Y18 phosphorylation (a fyn target) prevents the deleterious effects of tau on FAT. Similar experiments using the 6D tau isoform indicated that pseudophosphorylation at Y18 or T17 (and to a lesser extent Y29) prevents FAT inhibition, even when PAD is constitutively exposed. Further, we show that PAD exposure in AD brains occurs before Y18 phosphorylation and that a subset of PAD exposed tau is coincident with this modification, supporting the role of Y18 phosphorylation in mitigating the deleterious effects of PAD exposure in some of the tau pathology *in situ*. Together, these data suggest that the toxic effects of pathological tau species on FAT can be regulated via tyrosine kinase-mediated phosphorylation. Such findings have broad implications for the role of tau as a pathogenic factor in AD and other tauopathies.

Impaired axonal transport, as evidenced by numerous indirect measures (e.g. immunohistochemical and ultrastructural analyses of postmortem human tissue), has long been implicated in the pathogenesis of Alzheimer's disease (Dessi et al., 1997; Praprotnik et al., 1996; Stokin et al., 2005; Suzuki and Terry, 1967). Moreover, an association between FAT defects and pathogenic forms of tau has been implicated in AD and other neurodegenerative diseases (Morfini et al., 2002a; Morfini et al., 2009a; Roy et al., 2005), but the molecular basis was unclear. Studies using *in vitro* assays and tau overexpression in cultured cells suggested that tau impairs FAT by physically interfering with the binding of molecular motors to microtubules (Ebneth et al., 1998; Mandelkow et al., 2003; Vershinin et al., 2007). However, supraphysiological levels of tau not known to occur in AD were typically utilized in these studies making their biological relevance unclear. An experimental model was needed to allow precise control of tau levels and quantitative analysis of the effects on FAT. Isolated axoplasm from the squid giant axon provides a unique *ex vivo* model system that meets these criteria, and has additional advantages (Morfini et al., 2007a).

These advantages include: 1) the maintenance of functional anterograde and retrograde movement, 2) the maintenance of axoplasm organization and polarity, 3) the absence of protein and gene changes, and 4) molecular machinery that is highly conserved through humans. Using this model, we have shown that disease-associated tau species (e.g. tau filaments, AT8 tau, and an FTD mutant tau) inhibit anterograde FAT by activating a PP1-GSK3 cascade (LaPointe et al., 2009; Kanaan et al., in preparation, 2011).

Pathological observations in human tissue indicate that phosphorylation events (e.g. AT8) (Braak et al., 1994) and PAD exposure occur early during tau inclusion formation. Importantly, the abundance of TNT1 positive tau pathology in neuropil threads suggests PAD exposure occurs in both axons and dendrites. While the majority of our findings center around axonal transport, kinesin-based transport is important within both the soma and dendrites of neurons. Thus, the high levels of TNT1 positive tau in the somatodendritic compartment further highlight a role for PAD exposure in anterograde transport impairment in human disease. These findings suggest that the tau that is redistributed to the somatodendritic compartment in disease can negatively affect transport there as well.

Despite the presence of tau pathology, some neurons can survive for 2–3 decades bearing tau inclusions (Morsch et al., 1999). These findings raise an important question. How can some neurons mitigate the toxic effects of pathogenic tau, while others exhibit progressive pathology and degeneration? These issues imply the existence of regulatory mechanisms that affect the ability of PAD to inhibit FAT *in situ*. Tau is a well-known phosphoprotein that aggregates and becomes increasingly phosphorylated in AD and other tauopathies (Iqbal et al., 2005). In part, this reflects the activation of kinases as an element of AD pathogenesis (LaPointe et al., 2009; Morfini et al., 2002a; Pigino et al., 2009). Multiple disease-associated phosphorylation modifications can reduce tau's ability to bind microtubules and enhance or reduce the aggregation potential of tau *in vitro* (Sun and Gamblin, 2009). However, the functional implications of these phosphorylation modifications in the disease process have remained unclear in most cases.

Here, we provide direct evidence that phosphorylation within PAD blocks the deleterious effects of pathogenic tau on FAT. Both phosphorylation and pseudophosphorylation at Y18 in full-length WT tau filaments completely abolished their inhibitory effect on anterograde FAT. Furthermore, pseudophosphorylation at Y18 or T17 completely prevented 6D tau from inhibiting FAT. In our studies, the effects of pseudophosphorylation at Y29 on FAT were dependent on the form of tau tested. Tau filaments composed of Y29E tau significantly inhibited anterograde FAT much like WT tau filaments, while Y29E 6D tau partially reduced inhibition. The fact that Y29 is not within PAD, but is close in proximity, may explain this partial effect. Constraints imposed by sequences in full-length tau may explain why Y29E was not effective in preventing inhibition of anterograde FAT within full-length tau filaments.

Tyrosine 18 is of particular interest because it is a well characterized phosphorylation site for fyn (Lee et al., 2004) in a region of tau with significant divergence between primates and other organisms. In addition, pathologically aggregated tau is phosphorylated at Y18 in AD brains (Lee et al., 2004), and fyn kinase levels increase in neurons where fyn co-localizes with neurofibrillary tangles in AD (Ho et al., 2005; Shirazi and Wood, 1993). Fyn is a member of the src family of non-receptor tyrosine kinases that includes src, lyn and lck (Robinson et al., 2000), and tau is a substrate for many of these as well as other non-receptor tyrosine kinases (e.g. c-abl and syk) (Lebouvier et al., 2009; Lee, 2005). Collectively, these data suggest that non-receptor tyrosine kinases may play a role in reducing the toxic capacity of PAD exposure during disease pathogenesis (Fig. 8).

Highlighting the relevance of results obtained from studies in squid axoplasm, we found that Y18 phosphorylation occurs after PAD exposure in human brain tissue, and is mainly found in seemingly more mature tau inclusions in control brains. As AD progresses, both PAD exposure and phosphorylation at Y18 increase; however, the extent of phosphorylation at Y18 does not match the amount of tau pathology with PAD exposed. These data suggest that while Y18 phosphorylation may represent a compensatory mechanism aimed at rendering tau aggregates non-toxic in the brain, this mechanism is only partially effective. Additional mechanisms to reduce tau-mediated toxicity likely include modifications that block PAD by altering tau conformation (Jeganathan et al., 2006; Jeganathan et al., 2008) and/or N-terminal cleavage events that eliminate PAD (Horowitz et al., 2004).

The ability of fyn kinase to modify Y18 may be affected by a variety of factors. We show that fyn has a reduced ability to phosphorylate Y18 in pathological forms of tau including tau filaments, AT8 tau and an FTD mutant tau. Previously, a reduction in binding between fyn and tau on surface plasmon resonance assays was seen when 3 repeat tau was pseudophosphorylated at S199 and S202; however, pseudophosphorylated 4 repeat tau exhibited increased fyn binding (Bhaskar et al., 2005). Perhaps the additional modification at T205 reduces the interaction between 4 repeat tau and fyn leading to reduced Y18 phosphorylation in the current studies. Reduced levels of Y18 phosphorylation in Δ144–273 tau can be explained by the fact that all seven putative SH3 binding domains for docking fyn kinase are in the deleted region. Results from *in vitro* phosphorylation experiments here suggest that tau filaments and some disease-associated modifications of tau may impair phosphorylation at Y18 and prevent inactivation of PAD.

Our data, and those recently published (Ittner et al., 2010), suggest a complex relationship between fyn and the N-terminus of tau. Ittner and coworkers (2010) demonstrated that the N-terminus of tau is responsible for mediating the distribution of fyn kinase into dendritic spines. Interestingly, redistribution of tau, and subsequently fyn, to the soma reduced amyloid-β induced memory deficits and seizures in AD transgenic mice (Ittner et al., 2010). In light of our results, there are likely parallel functions of fyn that may depend upon cellular distribution and/or disease state. Although fyn may be localized to dendritic spines in a tau-dependent fashion where it can regulate synaptic function and excitotoxicity, fyn may also directly inactivate PAD-mediated FAT disruption as tau accumulates during disease progression (Fig. 8). Our data also provide insight into a potential role for Y18 phosphorylation by fyn (and other tyrosine kinases) in modulating PAD-mediated signaling under normal conditions for local cargo delivery (Fig. 8). Further investigations are required to understand functional relationships between tau and non-receptor tyrosine kinases more fully.

Identification of a mechanism for the toxic gain-of-function exhibited by tau filaments suggests that novel therapeutic approaches for AD and other tauopathies are feasible. Modulating the activities of PP1 and GSK3 is an obvious choice, but these enzymes are important in multiple pathways affecting many cellular processes (Avila and Hernandez, 2007; Cohen, 2002). The identification of PAD within the N-terminus of tau as a critical component in this gain of toxicity may provide a more specific target. Phosphorylation in this region (e.g. Y18) does not affect microtubule binding (Lee et al., 2004) or increase the aggregation potential of tau (Reynolds et al., 2005), which makes it an attractive site for intervention. Enhancing N-terminal phosphorylation and/or physically blocking or binding PAD could provide protection against the deleterious effects of pathogenic tau on FAT.

Supplementary Material

Refer to Web version on PubMed Central for supplementary material.

Acknowledgments

We would like to thank all of the members of the Brady and Morfini Labs who participated in our research at Woods Hole (Sarah Berth, Agnieszka Kaminska, Lisa Baker, Meryl Horn, Alex Sturbaum, John Bernstein and Maria Saparauskaite). In addition, we would like to thank Juan Reyes for some of the human tau samples and Yifan Fu for her assistance with generating the TNT1 antibody. This work was supported by NIH T32 AG020506-07 (NMK); NIH AG09466 (LIB); NIH NS23868, NS23320, NS41170 (STB); and ALS/CVS Therapy Alliance grant and 2007/2008 MBL Summer Research Fellowships (GM).

References

Avila J, Hernandez F. GSK-3 inhibitors for Alzheimer's disease. Expert Rev Neurother. 2007; 7:1527–1533. [PubMed: 17997701]

Berry RW, Sweet AP, Clark FA, Lagalwar S, Lapin BR, Wang T, Topgi S, Guillozet-Bongaarts AL, Cochran EJ, Bigio EH, Binder LI. Tau epitope display in progressive supranuclear palsy and corticobasal degeneration. J Neurocytol. 2004; 33:287–295. [PubMed: 15475684]

Bhaskar K, Yen SH, Lee G. Disease-related modifications in tau affect the interaction between Fyn and Tau. J Biol Chem. 2005; 280:35119–35125. [PubMed: 16115884]

Biernat J, Mandelkow EM, Schroter C, Lichtenberg-Kraag B, Steiner B, Berling B, Meyer H, Mercken M, Vandermeeren A, Goedert M. The switch of tau protein to an Alzheimer-like state includes the phosphorylation of two serine-proline motifs upstream of the microtubule binding region. EMBO J. 1992; 11:1593–1597. [PubMed: 1563356]

Bosco DA, Morfini G, Karabacak NM, Song Y, Gros-Louis F, Pasinelli P, Goolsby H, Fontaine BA, Lemay N, McKenna-Yasek D, Frosch MP, Agar JN, Julien JP, Brady ST, Brown RH Jr. Wild-type and mutant SOD1 share an aberrant conformation and a common pathogenic pathway in ALS. Nat Neurosci. 2010; 13:1396–1403. [PubMed: 20953194]

Braak E, Braak H, Mandelkow EM. A sequence of cytoskeleton changes related to the formation of neurofibrillary tangles and neuropil threads. Acta Neuropathol. 1994; 87:554–567. [PubMed: 7522386]

Brady ST, Richards BW, Leopold PL. Assay of vesicle motility in squid axoplasm. Methods Cell Biol. 1993; 39:191–202. [PubMed: 7504159]

Carmel G, Mager EM, Binder LI, Kuret J. The structural basis of monoclonal antibody Alz50's selectivity for Alzheimer's disease pathology. J Biol Chem. 1996; 271:32789–32795. [PubMed: 8955115]

Cohen PT. Protein phosphatase 1--targeted in many directions. J Cell Sci. 2002; 115:241–256. [PubMed: 11839776]

Dessi F, Colle M-A, Hauw J-J, Duyckaerts C. Accumulation of SNAP-25 immunoreactive material in axons of Alzheimer's disease. Neuroreport. 1997; 8:3685–3689. [PubMed: 9427351]

Ebneth A, Godemann R, Stamer K, Illenberger S, Trinczek B, Mandelkow E. Overexpression of tau protein inhibits kinesin-dependent trafficking of vesicles, mitochondria, and endoplasmic reticulum: implications for Alzheimer's disease. J Cell Biol. 1998; 143:777–794. [PubMed: 9813097]

Gamblin TC, King ME, Dawson H, Vitek MP, Kuret J, Berry RW, Binder LI. In vitro polymerization of tau protein monitored by laser light scattering: method and application to the study of FTDP-17 mutants. Biochemistry. 2000; 39:6136–6144. [PubMed: 10821687]

Giannakopoulos P, Herrmann FR, Bussiere T, Bouras C, Kovari E, Perl DP, Morrison JH, Gold G, Hof PR. Tangle and neuron numbers, but not amyloid load, predict cognitive status in Alzheimer's disease. Neurology. 2003; 60:1495–1500. [PubMed: 12743238]

Goedert M, Jakes R. Mutations causing neurodegenerative tauopathies. Biochim Biophys Acta. 2005; 1739:240–250. [PubMed: 15615642]

Goedert M, Jakes R, Vanmechelen E. Monoclonal antibody AT8 recognises tau protein phosphorylated at both serine 202 and threonine 205. Neurosci Lett. 1995; 189:167–169. [PubMed: 7624036]

Hasegawa M, Morishima-Kawashima M, Takio K, Suzuki M, Titani K, Ihara Y. Protein sequence and mass spectrometric analyses of tau in the Alzheimer's disease brain. J Biol Chem. 1992; 267:17047–17054. [PubMed: 1512244]

Ho GJ, Hashimoto M, Adame A, Izu M, Alford MF, Thal LJ, Hansen LA, Masliah E. Altered p59Fyn kinase expression accompanies disease progression in Alzheimer's disease: implications for its functional role. Neurobiol Aging. 2005; 26:625–635. [PubMed: 15708437]

Horowitz PM, LaPointe N, Guillozet-Bongaarts AL, Berry RW, Binder LI. N-terminal fragments of tau inhibit full-length tau polymerization in vitro. Biochemistry. 2006; 45:12859–12866. [PubMed: 17042504]

Horowitz PM, Patterson KR, Guillozet-Bongaarts AL, Reynolds MR, Carroll CA, Weintraub ST, Bennett DA, Cryns VL, Berry RW, Binder LI. Early N-terminal changes and caspase-6 cleavage of tau in Alzheimer's disease. J Neurosci. 2004; 24:7895–7902. [PubMed: 15356202]

Iqbal K, Alonso Adel C, Chen S, Chohan MO, El-Akkad E, Gong CX, Khatoon S, Li B, Liu F, Rahman A, Tanimukai H, Grundke-Iqbal I. Tau pathology in Alzheimer disease and other tauopathies. Biochim Biophys Acta. 2005; 1739:198–210. [PubMed: 15615638]

Ittner LM, Ke YD, Delerue F, Bi M, Gladbach A, van Eersel J, Wolfing H, Chieng BC, Christie MJ, Napier IA, Eckert A, Staufenbiel M, Hardeman E, Gotz J. Dendritic function of tau mediates amyloid-beta toxicity in Alzheimer's disease mouse models. Cell. 2010; 142:387–397. [PubMed: 20655099]

Jeganathan S, Hascher A, Chinnathambi S, Biernat J, Mandelkow EM, Mandelkow E. Proline-directed pseudo-phosphorylation at AT8 and PHF1 epitopes induces a compaction of the paperclip folding of Tau and generates a pathological (MC-1) conformation. J Biol Chem. 2008; 283:32066–32076. [PubMed: 18725412]

Jeganathan S, von Bergen M, Brutlach H, Steinhoff HJ, Mandelkow E. Global hairpin folding of tau in solution. Biochemistry. 2006; 45:2283–2293. [PubMed: 16475817]

King ME, Ahuja V, Binder LI, Kuret J. Ligand-dependent tau filament formation: implications for Alzheimer's disease progression. Biochemistry. 1999; 38:14851–14859. [PubMed: 10555967]

LaPointe NE, Morfini G, Pigino G, Gaisina IN, Kozikowski AP, Binder LI, Brady ST. The amino terminus of tau inhibits kinesin-dependent axonal transport: implications for filament toxicity. J Neurosci Res. 2009; 87:440–451. [PubMed: 18798283]

Lebouvier T, Scales TM, Williamson R, Noble W, Duyckaerts C, Hanger DP, Reynolds CH, Anderton BH, Derkinderen P. The microtubule-associated protein tau is also phosphorylated on tyrosine. J Alzheimers Dis. 2009; 18:1–9. [PubMed: 19542604]

Lee G. Tau and src family tyrosine kinases. Biochim Biophys Acta. 2005; 1739:323–330. [PubMed: 15615649]

Lee G, Newman ST, Gard DL, Band H, Panchamoorthy G. Tau interacts with src-family non-receptor tyrosine kinases. J Cell Sci. 1998; 111(Pt 21):3167–3177. [PubMed: 9763511]

Lee G, Thangavel R, Sharma VM, Litersky JM, Bhaskar K, Fang SM, Do LH, Andreadis A, Van Hoesen G, Ksiezak-Reding H. Phosphorylation of tau by fyn: implications for Alzheimer's disease. J Neurosci. 2004; 24:2304–2312. [PubMed: 14999081]

Luo MH, Tse SW, Memmott J, Andreadis A. Novel isoforms of tau that lack the microtubule-binding domain. J Neurochem. 2004; 90:340–351. [PubMed: 15228591]

Mandelkow EM, Stamer K, Vogel R, Thies E, Mandelkow E. Clogging of axons by tau, inhibition of axonal traffic and starvation of synapses. Neurobiol Aging. 2003; 24:1079–1085. [PubMed: 14643379]

Morfini G, Pigino G, Beffert U, Busciglio J, Brady ST. Fast axonal transport misregulation and Alzheimer's disease. Neuromolecular Med. 2002a; 2:89–99. [PubMed: 12428805]

Morfini G, Pigino G, Mizuno N, Kikkawa M, Brady ST. Tau binding to microtubules does not directly affect microtubule-based vesicle motility. J Neurosci Res. 2007a; 85:2620–2630. [PubMed: 17265463]

Morfini G, Pigino G, Opalach K, Serulle Y, Moreira JE, Sugimori M, Llinas RR, Brady ST. 1-Methyl-4-phenylpyridinium affects fast axonal transport by activation of caspase and protein kinase C. Proc Natl Acad Sci U S A. 2007b; 104:2442–2447. [PubMed: 17287338]

Morfini G, Szebenyi G, Brown H, Pant HC, Pigino G, DeBoer S, Beffert U, Brady ST. A novel CDK5-dependent pathway for regulating GSK3 activity and kinesin-driven motility in neurons. EMBO J. 2004; 23:2235–2245. [PubMed: 15152189]

Morfini G, Szebenyi G, Elluru R, Ratner N, Brady ST. Glycogen synthase kinase 3 phosphorylates kinesin light chains and negatively regulates kinesin-based motility. EMBO J. 2002b; 21:281–293. [PubMed: 11823421]

Morfini GA, Burns M, Binder LI, Kanaan NM, LaPointe N, Bosco DA, Brown RH Jr, Brown H, Tiwari A, Hayward L, Edgar J, Nave KA, Garberrn J, Atagi Y, Song Y, Pigino G, Brady ST. Axonal transport defects in neurodegenerative diseases. J Neurosci. 2009a; 29:12776–12786. [PubMed: 19828789]

Morfini GA, You YM, Pollema SL, Kaminska A, Liu K, Yoshioka K, Bjorkblom B, Coffey ET, Bagnato C, Han D, Huang CF, Banker G, Pigino G, Brady ST. Pathogenic huntingtin inhibits fast axonal transport by activating JNK3 and phosphorylating kinesin. Nat Neurosci. 2009b; 12:864–871. [PubMed: 19525941]

Morsch R, Simon W, Coleman PD. Neurons may live for decades with neurofibrillary tangles. J Neuropathol Exp Neurol. 1999; 58:188–197. [PubMed: 10029101]

Pigino G, Morfini G, Atagi Y, Deshpande A, Yu C, Jungbauer L, LaDu M, Busciglio J, Brady S. Disruption of fast axonal transport is a pathogenic mechanism for intraneuronal amyloid beta. Proc Natl Acad Sci U S A. 2009; 106:5907–5912. [PubMed: 19321417]

Pollock NJ, Mirra SS, Binder LI, Hansen LA, Wood JG. Filamentous aggregates in Pick's disease, progressive supranuclear palsy, and Alzheimer's disease share antigenic determinants with microtubule-associated protein, tau. Lancet. 1986; 2:1211. [PubMed: 2430155]

Praprotnik D, Smith MA, Richey PL, Vinters HV, Perry G. Filament heterogeneity within the dystrophic neurites of senile plaques suggests blockage of fast axonal transport in Alzheimer's disease. Acta Neuropathol. 1996; 91:226–235. [PubMed: 8834534]

Price DL, Wong PC, Borchelt DR, Pardo CA, Thinakaran G, Doan AP, Lee MK, Martin LJ, Sisodia SS. Amyotrophic lateral sclerosis and Alzheimer disease. Lessons from model systems. Rev Neurol (Paris). 1997; 153:484–495. [PubMed: 9683997]

Reyes JF, Reynolds MR, Horowitz PM, Fu Y, Guillozet-Bongaarts AL, Berry R, Binder LI. A possible link between astrocyte activation and tau nitration in Alzheimer's disease. Neurobiol Dis. 2008; 31:198–208. [PubMed: 18562203]

Reynolds MR, Berry RW, Binder LI. Site-specific nitration and oxidative dityrosine bridging of the tau protein by peroxynitrite: implications for Alzheimer's disease. Biochemistry. 2005; 44:1690–1700. [PubMed: 15683253]

Reynolds MR, Reyes JF, Fu Y, Bigio EH, Guillozet-Bongaarts AL, Berry RW, Binder LI. Tau nitration occurs at tyrosine 29 in the fibrillar lesions of Alzheimer's disease and other tauopathies. J. Neurosci. 2006; 26:10636–10645. [PubMed: 17050703]

Robinson DR, Wu YM, Lin SF. The protein tyrosine kinase family of the human genome. Oncogene. 2000; 19:5548–5557. [PubMed: 11114734]

Rovelet-Lecrux A, Lecourtois M, Thomas-Anterion C, Le Ber I, Brice A, Frebourg T, Hannequin D, Campion D. Partial deletion of the MAPT gene: a novel mechanism of FTDP-17. Hum Mutat. 2009; 30:E591–E602. [PubMed: 19263483]

Roy S, Zhang B, Lee VM, Trojanowski JQ. Axonal transport defects: a common theme in neurodegenerative diseases. Acta Neuropathol. 2005; 109:5–13. [PubMed: 15645263]

Shirazi SK, Wood JG. The protein tyrosine kinase, fyn, in Alzheimer's disease pathology. Neuroreport. 1993; 4:435–437. [PubMed: 8388744]

Solowska JM, Morfini G, Falnikar A, Himes BT, Brady ST, Huang D, Baas PW. Quantitative and functional analyses of spastin in the nervous system: implications for hereditary spastic paraplegia. J Neurosci. 2008; 28:2147–2157. [PubMed: 18305248]

Stokin GB, Lillo C, Falzone TL, Brusch RG, Rockenstein E, Mount SL, Raman R, Davies P, Masliah E, Williams DS, Goldstein LSB. Axonopathy and transport deficits early in the pathogenesis of Alzheimer's disease. Science. 2005; 307:1282–1288. [PubMed: 15731448]

Sun Q, Gamblin TC. Pseudohyperphosphorylation causing AD-like changes in tau has significant effects on its polymerization. Biochemistry. 2009; 48:6002–6011. [PubMed: 19459590]

Suzuki K, Terry RD. Fine structural localization of acid phosphatase in senile plaques in Alzheimer's presenile dementia. Acta Neuropathol. 1967; 8:276–284. [PubMed: 6039977]

Vershinin M, Carter BC, Razafsky DS, King SJ, Gross SP. Multiple-motor based transport and its regulation by Tau. Proc Natl Acad Sci U S A. 2007; 104:87–92. [PubMed: 17190808]

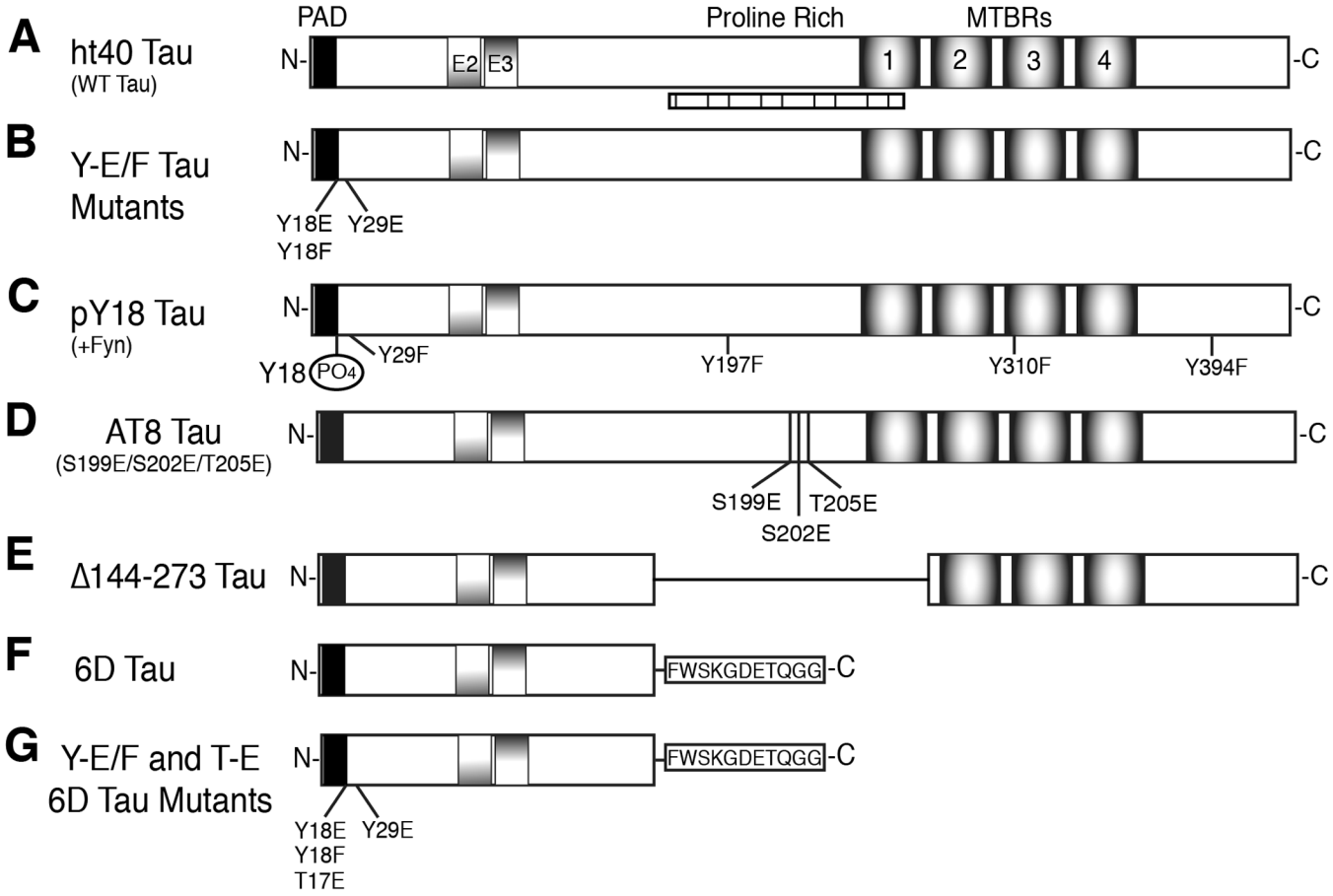

Fig. 1.

Schematic diagram of tau constructs used. (A) The longest human adult isoform of tau, ht40 (WT tau), contains exons 2 and 3 (E2 and E3) and four MTBRs. PAD (AEPRQEFEVMEDHAGTY) is responsible for inhibiting anterograde FAT (black box). Seven putative SH3 binding domains exist in tau between amino acids 176–236 (vertically hatched box) (Lee et al., 1998). (B) The Y→E/F tau mutants are full-length tau constructs with single pseudophosphorylation mutations (E – glutamic acid) at Y18 or Y29. A mutation control protein consisted of a Y→F (phenylalanine) mutation at residue 18. (C) The pY18 tau protein is full-length tau phosphorylated specifically at Y18 by fyn kinase. To ensure that only Y18 was phosphorylated by fyn, all of the other tyrosines in tau (Y29, Y197, Y310, and Y394) were mutated to F. (D) The AT8 tau protein was pseudophosphorylated at S199, S202 and T205 by mutagenesis of S→E and T→E to mimic the phosphoepitope recognized by the AT8 antibody (Biernat et al., 1992; Goedert et al., 1995) in hyperphosphorylated tau. (E) The Δ144–273 mutation contains a deletion of amino acids 144–273 (the proline-rich region and MTBR1), which was found in a patient with an autosomal dominant familial form of FTD (Rovelet-Lecrux et al., 2009). (F) 6D tau is a truncated, non-canonical N-terminal isoform resulting from alternative splicing in exon 6 and containing a unique 11 amino acid C-terminal sequence (in box). (G) Single pseudophosphorylation mutants of 6D tau were generated at Y18E, Y29E, and T17E. The Y18F 6D mutant protein was used as a mutation control.

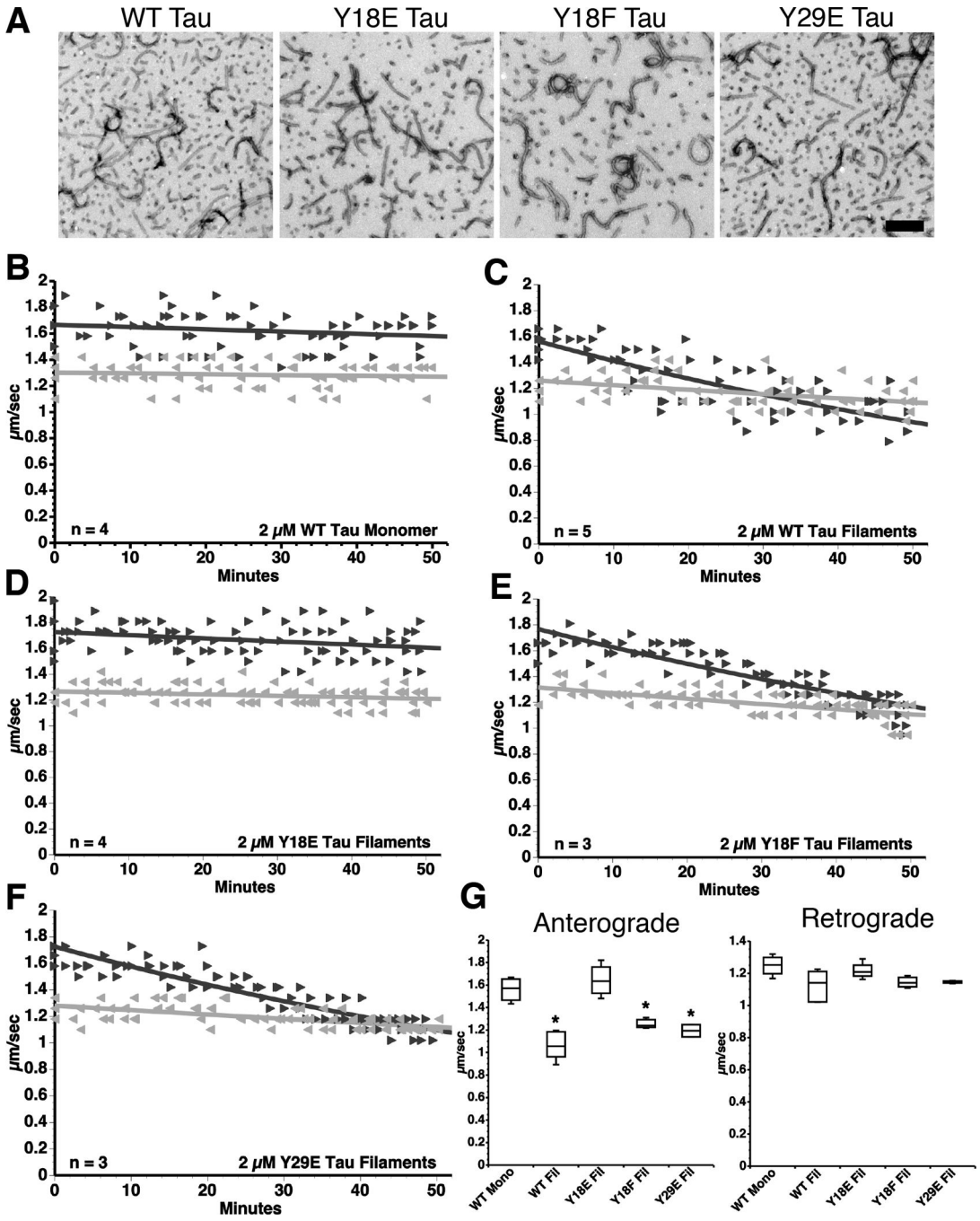

Fig. 2.

Pseudophosphorylation of Y18 prevents tau filaments from inhibiting anterograde FAT. (A) Representative electron micrographs illustrate that WT tau, Y18E tau, Y18F tau and Y29E tau produced comparable quantities of morphologically similar filaments (see Supplementary Fig. S1A). Scale bar = 250 nm. (B–F) Vesicle motility assays in isolated squid axoplasm. Individual velocity (μm/sec) measurements (arrowheads) are plotted as a function of time (minutes). (B) Perfusion of WT tau monomers did not affect anterograde (►) or retrograde (◄) FAT rates. (C) In contrast, perfusion of WT tau filaments selectively inhibited anterograde, but not retrograde FAT. (D) Filaments composed of Y18E tau did not

affect FAT. (E) Y18F tau filaments (a non-phosphomimicking control mutation) selectively inhibited anterograde FAT (see Supplementary Fig. S1B). (F) Y29E tau filaments specifically decreased anterograde FAT. (G) Quantification of anterograde and retrograde FAT rates in B–F indicates that WT, Y18F and Y29E filaments significantly reduce the rate of anterograde FAT relative to WT tau monomers in isolated axoplasms (one-way ANOVA; * $p<0.01$). Retrograde FAT was unaffected by all tau constructs tested.

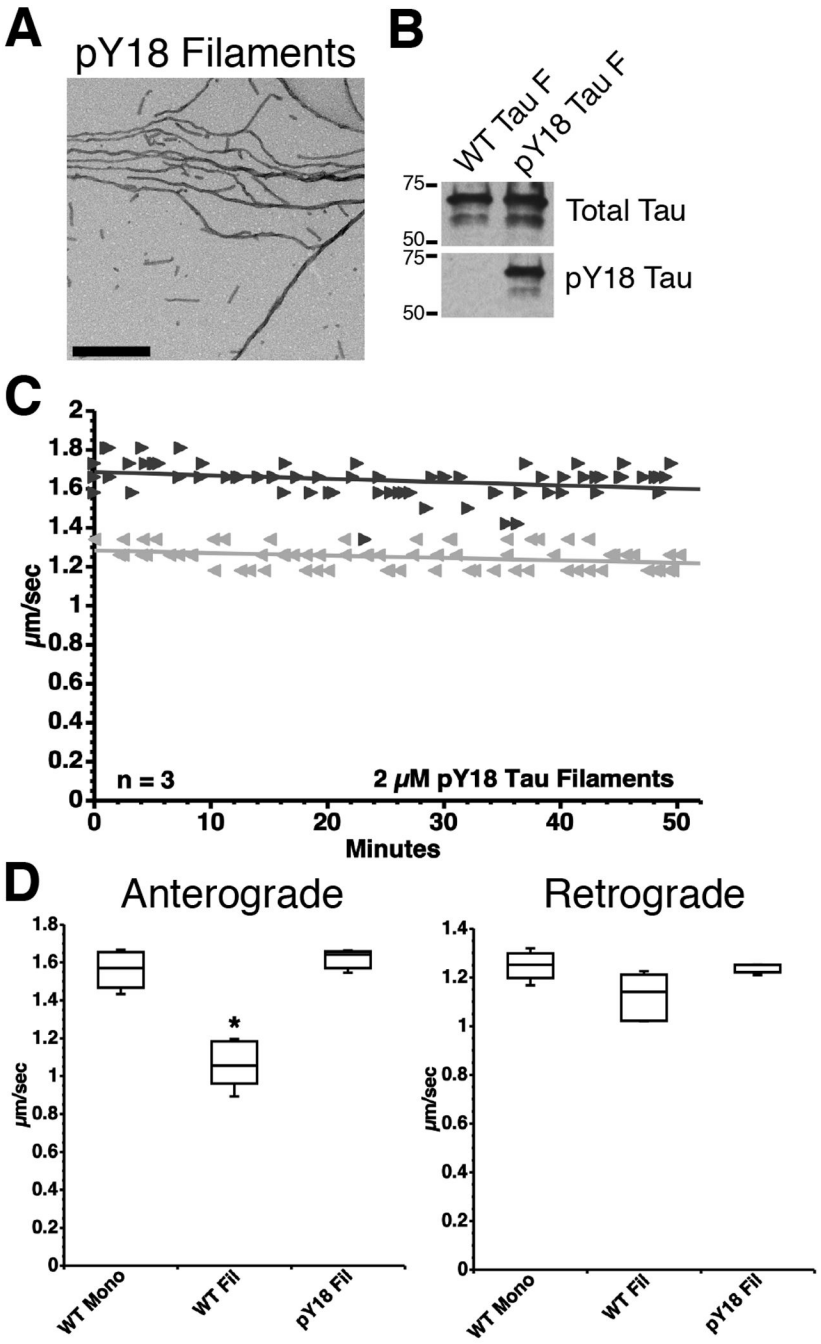

Fig. 3.

Fyn-mediated phosphorylation of Y18 prevents the inhibitory effect of tau filaments on anterograde FAT. (A) A tau mutant with a single Y at position 18 (all other tyrosines were mutated to F) was incubated with fyn kinase to phosphorylate Y18 (pY18 tau) prior to polymerization. An electron micrograph confirming that pY18 tau can polymerize into filaments. Scale bar = 500 nm. (B) Immunoblots using the phosphorylation-independent R1 tau antibody (total tau) and the 9G3 antibody, a phospho-Y18-specific antibody, confirmed the phosphorylation status of Y18 in the filaments used in motility assays (shown in panel C; see Supplementary Fig. 2). (C) Unlike WT tau filaments (Fig. 2C), pY18 tau filaments had

no effect on FAT (► anterograde; ◄ retrograde). (D) Box plots summarizing the statistical comparisons of data shown in panel C (one-way ANOVA; * $p<0.01$ compared to WT tau monomer and pY18 tau filaments).

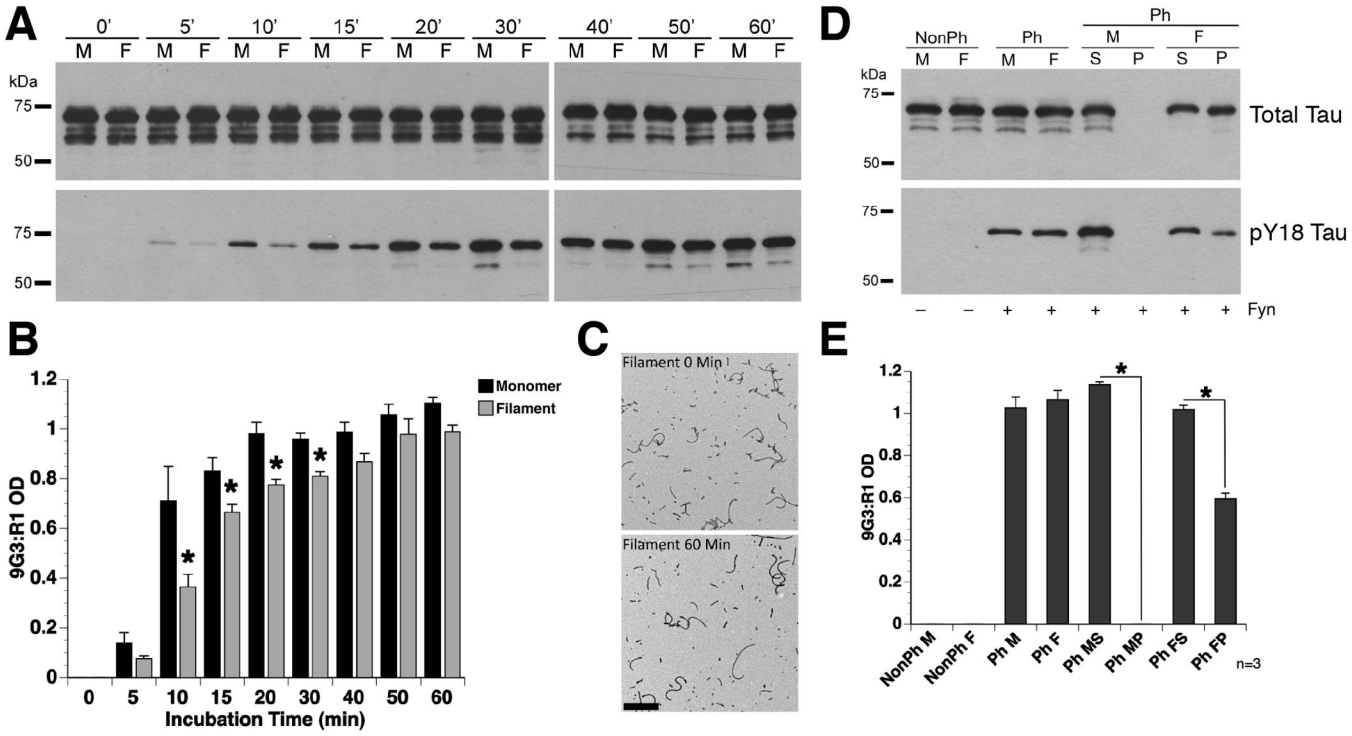

Fig. 4.

Tau monomers are more readily phosphorylated than tau filaments at Y18. (A) Representative blots of *in vitro* kinase reactions (0–60 minute incubation) using fyn kinase with either WT tau monomer (M) or filaments (F). Antibodies used were R1 for total tau and 9G3 for pY18 tau. (B) Quantification of Y18 phosphorylation demonstrated an increased rate of phosphorylation in tau monomers, when compared to tau filaments (two-way repeated measure ANOVA; * $p<0.05$; error bars = +SEM). (C) Representative electron micrographs of tau filaments taken at 0 and 60 minutes after incubation with fyn kinase confirmed that tau filaments did not depolymerize upon phosphorylation at Y18. Scale bar = 500 nm. (D) Representative blots of a spin down assay performed after 10 minutes incubation with fyn kinase suggest that phosphates were added to tau proteins incorporated into the pre-formed tau filaments. (NonPh – prior to fyn incubation; Ph – post fyn incubation; S – soluble fraction; P – pellet fraction). (**E**) Quantification of pY18 reactivity demonstrates that pelleted tau filaments (PhFP) were phosphorylated at Y18, but at levels ~40% lower than soluble tau in the polymerized sample (PhFS). The monomeric tau sample (PhMS and PhMP) confirms the efficacy of separating soluble monomers from filamentous tau species since no monomeric tau was present in the pelleted fraction (two-way ANOVA; * $p<0.05$; error bars = +SEM).

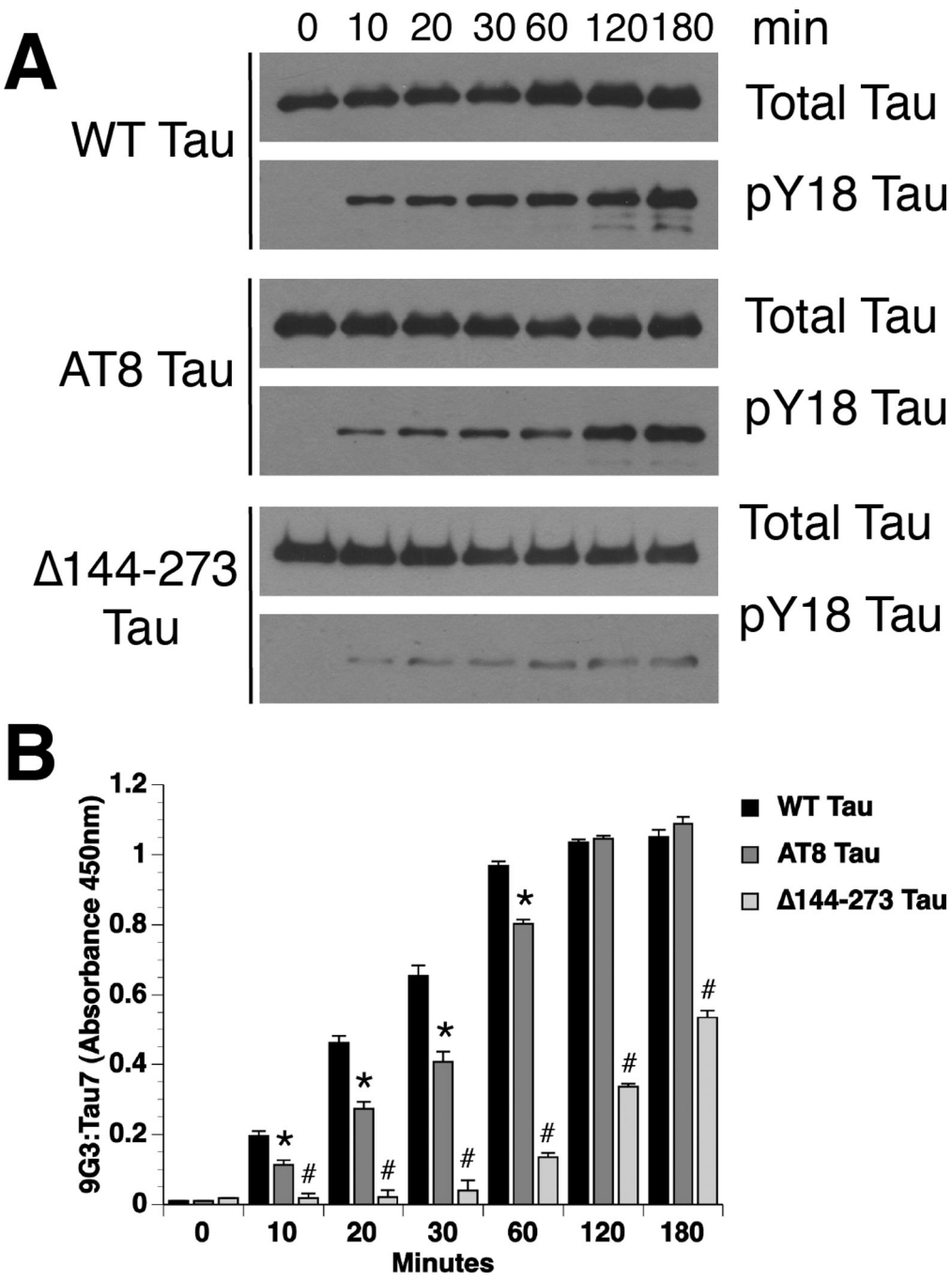

Fig. 5.

Disease-associated tau modifications impair phosphorylation at Y18. (A) WT tau was rapidly phosphorylated at Y18 by fyn kinase. In contrast, fyn-mediated phosphorylation of Y18 in AT8 tau and Δ144–273 tau was reduced. Antibodies used were Tau7 for total tau and 9G3 for pY18 tau. (B) Analysis of pY18 tau levels by ELISA demonstrates that while the maximal level of phosphorylation was similar, the rate of Y18 phosphorylation in AT8 tau was significantly reduced compared to WT tau (two-way repeated measure ANOVA; * $p<0.05$ compared to WT tau). Both the rate and maximal level of phosphorylation at Y18 in Δ144–273 tau was dramatically reduced compared to WT tau and AT8 tau (# $p<0.05$ compared to WT and AT8 tau).

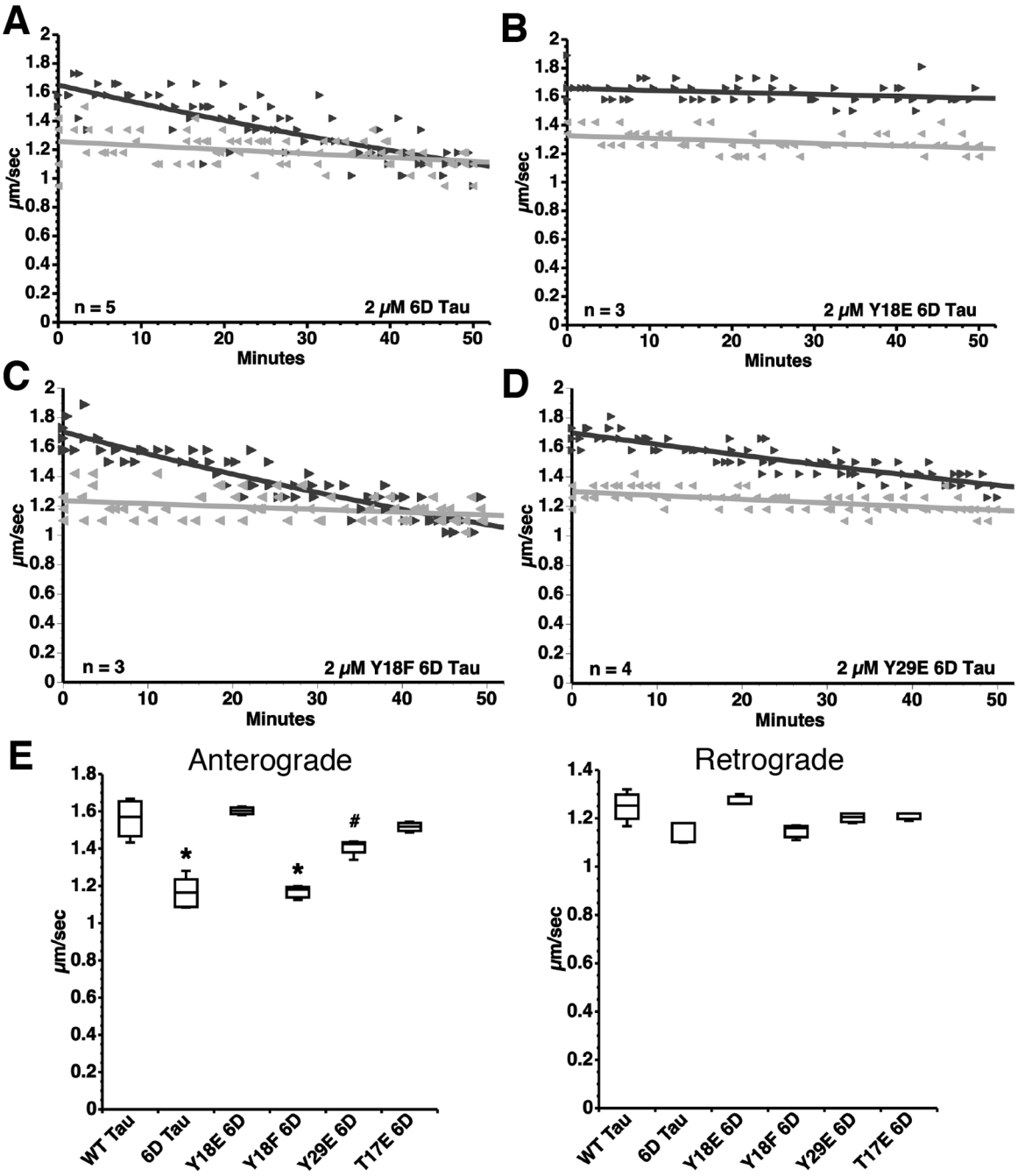

Fig. 6.

Y18 pseudophosphorylation prevents the inhibitory effect of 6D tau on anterograde FAT. (A) Perfusion of 6D tau inhibits anterograde FAT (►) without affecting retrograde FAT (◄). (B) Pseudophosphorylation at Y18 in 6D tau (Y18E) prevents this effect. (C) Perfusion of Y18F 6D tau inhibits anterograde FAT to an extent comparable to 6D tau. (D) Perfusion of Y29E 6D tau inhibits anterograde FAT to a lesser extent than 6D tau. (E) Box plots summarizing the data shown in panels A–D and the statistical comparisons (one-way ANOVA; * $p<0.01$ compared to WT tau, Y18E 6D, Y29E 6D and T17E 6D; # $p<0.01$ compared to Y18E 6D) (see also Supplementary Fig. S4).

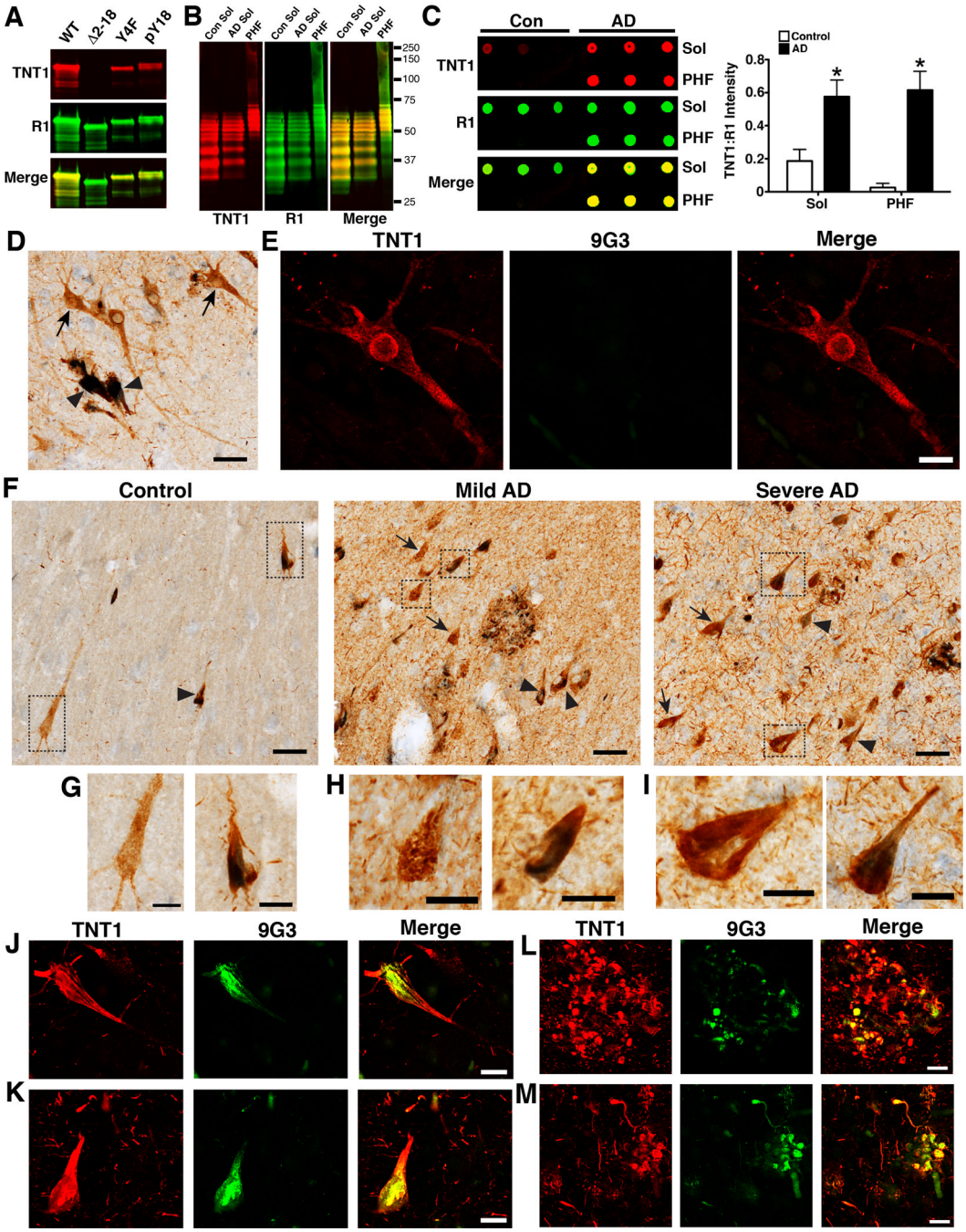

Fig. 7.

PAD exposure precedes and is more abundant than Y18 phosphorylation in human brains. (A) The specificity of TNT1 (red) for PAD was tested by Western blot using recombinant WT tau and Δ2–18 tau. Additionally, phosphorylation at Y18 does not interfere with TNT1 reactivity (red) as indicated by similar reactivity between Y4F and pY18 Y4F tau. (B–C) The specificity of TNT1 for tau proteins was confirmed using soluble (Sol) and insoluble (PHF) fractions isolated from the frontal cortex of control (n=3) and AD (n=3) brains. (B) Note that in *denaturing conditions* on Western blots TNT1 (red) reacts with all tau samples from controls and AD brains. (C) However, when samples were run in *non-denaturing conditions* on dot blots TNT1 (red) shows remarkable selectivity for soluble and insoluble

tau from AD brains, not from controls. In A–C, R1 (green) was used to label total tau. (D) Immunohistochemistry for PAD exposed tau (TNT1 positive, brown) and phospho-Y18 tau (9G3 positive, blue) in controls (Braak stages I–II) reveals that Y18 phosphorylation occurs in more mature compact TNT1 positive tau inclusions (▸), rather than the early stage of tau accumulation indicated by diffuse cytoplasmic staining in "pre-tangle" neurons (→). Scale bars are 50μm. (E) Immunofluorescence confirmed the lack of phospho-Y18 tau (green) in the early pre-tangle neurons that are diffusely stained with TNT1 (red) in control brains (Braak stages I–II). Scale bars are 20μm. (F) Immunohistochemistry in hippocampal sections shows that TNT1 pathology (brown) is substantially increased in mild AD (Braak stages III–IV) and severe AD (Braak stages V–VI), compared to control cases (Braak stages I–II). The 9G3 positive pathology (blue) does increase with disease severity but not to the same magnitude as TNT1. Additionally, 9G3 shows nearly complete co-localization with TNT1 in all stages (TNT1+ neurons →; TNT1+9G3 neurons ▸). Scale bars are 50μm. (G–I) High magnification of the boxed images in (F) depict single (TNT1 only; brown) and double stained (TNT+ 9G3; brown and blue) neurons in control (G), mild AD (H) and severe AD (I) cases. Scale bars are 20μm. (J–M) Immunofluorescence confirmed the co-localization of TNT1 (red) and 9G3 (green) in hippocampal neurons containing mature compact tau inclusions from control (J) and severe AD (K) cases. Neuritic plaques consistently exhibit co-localization of TNT1 and 9G3 in mild (L) and severe AD (M), but TNT1 immunoreactivity is more extensive. Scale bars are 20μm.

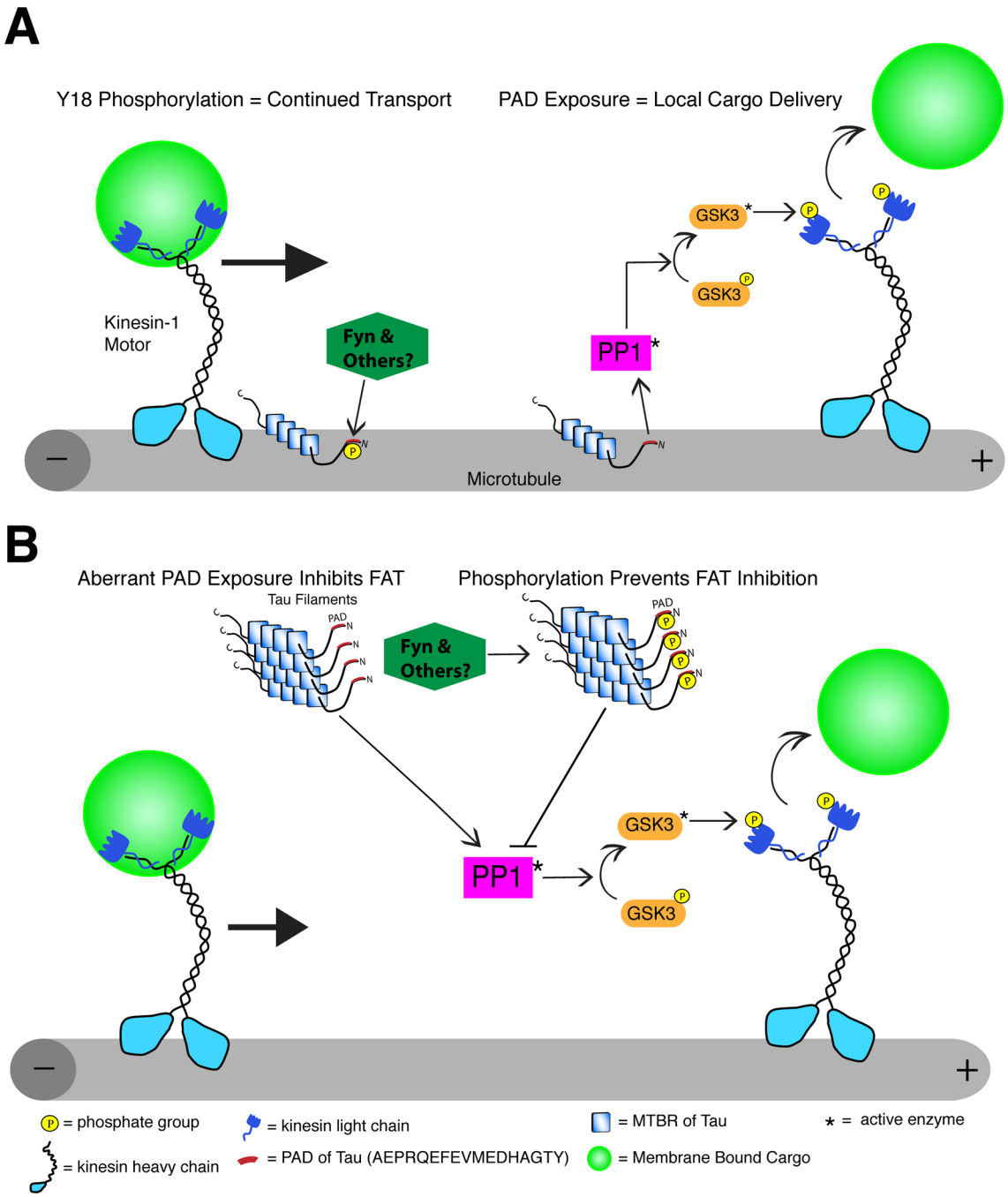

Fig. 8.

Schematic diagram of the proposed role for N-terminal phosphorylation of tau in cargo delivery and aberrant inhibition of anterograde FAT in disease. (A) Normally, tau localizes to microtubules where, in addition to stabilizing microtubules, it is capable of regulating local cargo delivery through PAD-mediated activation of the PP1-GSK3 cascade. Under normal conditions, cargoes are transported by conventional kinesin along microtubules when tau is phosphorylated at Y18 (by fyn or other tyrosine kinasaes) because PAD cannot activate the PP1-GSK3 cascade. In contrast, cargo is delivered at locations where intact unmodified PAD is exposed. (B) In disease, tau aggregation and other modifications expose PAD in tau no longer attached to microtubules, which initiates aberrant activation of the

PP1-GSK3 cascade, inhibition of anterograde FAT and ultimately neuron dysfunction/degeneration. Neurons can mitigate the effects of abnormal PAD presentation in disease-modified tau species through Y18 phosphorylation (by fyn or other tyrosine kinases), which renders pathogenic tau non-toxic to FAT.